Molecular Imaging with ^{123}I-FIAU, ^{18}F-FUdR, ^{18}F-FET, and ^{18}F-FDG for Monitoring Herpes Simplex Virus Type 1 Thymidine Kinase and Ganciclovir Prodrug Activation Gene Therapy of Cancer

Hsin-Ell Wang[1], Hung-Man Yu[1], Ren-Shyan Liu[2,3], Mai Lin[1], Juri G. Gelovani[4], Jeng-Jong Hwang[1], Hon-Jian Wei[5], and Win-Ping Deng[5]

[1]Institute of Radiological Science, National Yang-Ming University, Taipei, Taiwan; [2]Department of Nuclear Medicine and National PET Cyclotron Center, Veterans General Hospital, Taipei, Taiwan; [3]Department of Nuclear Medicine, School of Medicine, National Yang-Ming University, Taipei, Taiwan; [4]Department of Experimental Diagnostic Imaging, M.D. Anderson Cancer Center, Houston, Texas; and [5]Institute of Biomedical Materials, Taipei Medical University, Taipei, Taiwan

The ability to monitor tumor responses during prodrug activation gene therapy and other anticancer gene therapies is critical for their translation into clinical practice. Previously, we demonstrated the feasibility of noninvasive in vivo imaging with ^{131}I-5-iodo-2′-fluoro-1-β-D-arabinofuranosyluracil (^{131}I-FIAU) for monitoring herpes simplex virus type 1 thymidine kinase (*HSV1-tk*) cancer gene expression in an experimental animal model. Here we tested the efficacy of SPECT with ^{123}I-FIAU and PET with 5-^{18}F-fluoro-2′-deoxyuridine (^{18}F-FUdR), 2-^{18}F-fluoroethyl-L-tyrosine (^{18}F-FET), and ^{18}F-FDG for monitoring tumor responses during prodrug activation gene therapy with *HSV1-tk* and ganciclovir (GCV). **Methods:** In the flanks of FVB/N female mice, 4 tumors per animal were established by subcutaneous injection of 1×10^5 cells of NG4TL4 sarcoma cells, *HSV1-tk*–transduced NG4TL4-STK cells, or a mixture of these cells in different proportions to model different efficacies of transfection and *HSV1-tk* gene expression levels in tumors. Ten days later, the animals were treated with GCV (10 mg/kg/d intraperitoneally) for 7 d. γ-Imaging with ^{123}I-FIAU and PET with ^{18}F-FUdR, ^{18}F-FET, and ^{18}F-FDG were performed before and after initiation of therapy with GCV in the same animal. **Results:** Before GCV treatment, no significant difference in weight and size was found in tumors that expressed different *HSV1-tk* levels, suggesting similar in vivo proliferation rates for NG4TL4 and NG4TL4-STK sarcomas. The accumulation of ^{123}I-FIAU at 24 h after injection was directly proportional to the percentage of NG4TL4-STK cells in the tumors. The ^{123}I-FIAU accumulation at 4 and 7 d of GCV therapy decreased significantly compared with pretreatment levels and was proportional to the percentage of *HSV1-tk*–positive tumor cells. Tumor uptake of ^{18}F-FUdR in all *HSV1-tk*–expressing tumors also decreased significantly compared with pretreatment levels and was proportional to the percentage of *HSV1-tk*–positive tumor cells. The accumulation of ^{18}F-FET decreased minimally (about 1.5-fold) and ^{18}F-FDG decreased only 2-fold after 7 d of GCV therapy, and the degree of reduction was proportional to the percentage of *HSV1-tk*–positive tumor cells. **Conclusion:** We have shown that γ-camera imaging with ^{123}I-FIAU was the most reliable method for prediction of tumor response to GCV therapy, which was proportional to the magnitude of *HSV1-tk* expression in tumor tissue. ^{123}I-FIAU imaging can be used to verify the efficacy of elimination of *HSV1-tk*–expressing cells by therapy with GCV. PET with ^{18}F-FUdR reliably visualizes proliferating tumor tissue and is most suitable for the assessment of responses in tumors undergoing *HSV1-tk* plus GCV prodrug activation gene therapy. PET with ^{18}F-FDG or ^{18}F-FET can be used as additional "surrogate" biomarkers of the treatment response, although these radiotracers are less sensitive than ^{18}F-FUdR for monitoring tumor responses to prodrug activation gene therapy with *HSV1-tk* and GCV in this sarcoma model.

Key Words: ^{123}I-FIAU; ^{18}F-FDG; ^{18}F-FUdR; ^{18}F-FET; microPET; gene therapy; herpes simplex virus thymidine kinase; ganciclovir; tumor

J Nucl Med 2006; 47:1161–1171

Conventional modalities for treatment of cancer, such as surgery, chemotherapy, and radiotherapy, fail to achieve cures in a significant number of cancer patients. Prodrug activation or "suicide" gene therapy of cancer has been intensively investigated over the past 2 decades (*1*). Introduction of the herpes simplex virus type 1 thymidine kinase (*HSV1-tk*) gene into tumor cells makes these cells sensitive to antiviral drugs, such as ganciclovir (GCV) (*2*). *HSV1-tk* phosphorylates GCV to monophosphate, which is subsequently phosphorylated by host kinases, and eventually

Received May 18, 2005; revision accepted Mar. 31, 2006.

For correspondence or reprints contact: Win-Ping Deng, PhD, Institute of Biomedical Materials, Taipei Medical University, 250, Wu-Hsing St., Taipei 110, Taiwan.

E-mail: wpdeng@ms41.hinet.net

leads to death not only of the transfected tumor cells but also of neighboring nontransfected cells (*3*). The potential of *HSV1-tk* suicide gene therapy has been demonstrated in animal studies, in which complete eradication of the tumor was observed (*2,4*). Despite of these promising preclinical results, the first clinical trials for brain tumors with *HSV1-tk*/GCV gene therapy showed discouraging therapeutic responses (*5*).

PET and SPECT techniques are routinely used for detection and monitoring therapy of cancer. The ability to detect the location, magnitude, and duration of gene expression quantitatively and noninvasively represents big progress in the objective evaluation of gene therapy. The expression of a transfected gene can be imaged in vivo by using an appropriate combination of "reporter gene" and "reporter substrate". Various substrates of the HSV1-tk enzyme have now been radiolabeled with positron-emitting isotopes, including ^{124}I-5-iodo-2′-fluoro-1-β-D-arabinofuranosyluracil (^{124}I-FIAU) (*6,7*), ^{18}F-9-[4-fluoro-3-(hydroxymethyl)butyl]-guanine (^{18}F-FHBG) (*8*), ^{18}F-2′-fluoro-1-β-D-arabinofuranosyl-5-ethyl-uracil (^{18}F-FEAU) (*9,10*), and other 2′-fluoro 5-substituted pyrimidine nucleoside analogs (*11*).

High efficiency of gene transfer is important for achieving adequate responses to gene therapy in clinical trials. Previously, we have used ^{131}I- and ^{124}I-FIAU for imaging with SPECT and PET, respectively, and demonstrated the feasibility of these radiotracers for noninvasive monitoring of cancer gene therapy in experimental animal models of *HSV1-tk*–expressing tumors (*6,12–14*). Successful imaging of *HSV1-tk* expression in a human gene therapy trial was reported for the first time using ^{124}I-FIAU PET (*15*) and more recently using ^{18}F-FHBG (*16*).

However, the feasibility of noninvasive imaging-based assessment of the overall tumor response to prodrug activation gene therapy has not been studied in detail. Only a limited number of reports have described changes in tumor glucose metabolism, amino acid metabolism, and proliferative activity during *HSV1-tk* plus GCV prodrug activation gene therapy in preclinical (*17–19*) and clinical studies (*16,20*).

PET with several molecular imaging agents could be applicable for monitoring tumor responses to prodrug activation gene therapy of cancer. ^{18}F-FDG has proven useful as a PET agent in oncology (*21,22*). ^{18}F-FDG is metabolically trapped in tissues after phosphorylation by hexokinase instead of a natural substrate during glycolysis. However, high ^{18}F-FDG uptake in other pathophysiologic conditions such as inflammation and infection (*23,24*) results in an inadequately low specificity of ^{18}F-FDG imaging for tumor detection and therapy monitoring. Nevertheless, ^{18}F-FDG has been widely applied for monitoring anticancer therapies in the clinic (*25,26*).

Amino acids are essential for protein synthesis and growth of tumor cells, in which both the amino transport and the protein synthesis rate are upregulated. Several radiolabeled amino acid analogs, including 2-^{18}F-fluoroethyl-L-tyrosine (^{18}F-FET), have been developed for diagnostic PET of brain tumors and for differentiation of recurrence from radiation necrosis (*27,28*). ^{18}F-FET was recently compared with ^{18}F-FDG for detection of non–central nervous system malignancies (*29*).

Nucleosides are essential for cell proliferation and their radiolabeled analogs can be used to discriminate between normal tissues and rapidly proliferating malignancies. The 5-^{18}F-fluoro-2′-deoxyuridine (^{18}F-FUdR) is phosphorylated by the host uridine kinase to FUdR monophosphate, which acts as an irreversible inhibitor of thymidylate synthase and is entrapped within the target cell (*30,31*). Therefore, in the current study, in addition to ^{123}I-FIAU for SPECT imaging of *HSV1-tk* expression, we used PET imaging with ^{18}F-FDG, ^{18}F-FET, and ^{18}F-FUdR to assess changes in tumor glucose and amino acid metabolism and proliferation, respectively, as surrogate biomarkers of *HSV1-tk* plus GCV suicide gene therapy of a sarcoma model in mice.

MATERIALS AND METHODS

Chemicals

5-Iodo-2′-deoxyurdine (IUdR) and FIAU were purchased from Sigma. 3,4-Dihydropyran (DHP) was purchased from Acros. Acetic anhydride, hexabutylditin $(Bu_3Sn)_2$, potassium carbonate, ethylene glycol, *p*-toluenesulfonyl chloride, anhydrous acetonitrile, and other chemicals were purchased from Merck and Co., Inc. All solvents were dried before use by distillation from sodium or calcium hydride. GCV was purchased from Roche, Inc. Minimum essential medium (MEM), fetal bovine serum (FBS), and geneticin (G418) were purchased from Life Technologies, Inc.

Synthesis of ^{18}F-FUdR

Preparation of 3′,5′-Di-O-Acetyl-5-Iodo-2′-Deoxyuridine (IUdR-$(OAc)_2$). IUdR-$(OAc)_2$ was synthesized by acetylation of 5-iodo-2′-deoxyuridine (1 g, 2.29 mmol) with acetic anhydride (2 mL) in pyridine (10 mL) at ambient temperature for 30 min. The solvent was removed by vacuum. Diethyl ether was added for precipitation. The white precipitate was collected, redistributed in water, and then extracted with chloroform. The solvent was removed by rotary evaporator and recrystallized in diethyl ether and chloroform to obtain IUdR-$(OAc)_2$ as white solid crystals (1.13 g, 1.88 mmol, 82% yield).

Preparation of 3′,5′-Di-O-Acetyl-5-Tributylstannyl-2′-Deoxyuridine (Bu_3SnUdR-$(OAc)_2$). IUdR-$(OAc)_2$ (0.5 g, 1.14 mmol) was dissolved in anhydrous 1,4-dioxane (20 mL). Bis(triphenylphosphine) palladium(II) chloride ($(PPh_3)_2PdCl_2$) (20 mg) and $(Bu_3Sn)_2$ (1.74 g, 3 mmol) were added. The mixture was heated at 120°C for 5 h under a stream of nitrogen. After cooling, the solvent was removed by rotary evaporation. The mixture was separated by column chromatography (ethyl acetate/chloroform = 20:80, silica gel adsorbent) to give the ^{18}F-FUdR precursor Bu_3SnUdR-$(OAc)_2$ as a pale yellow oil (0.4 g, 0.62 mmol, 58% yield).

^{18}F-Fluorination. ^{18}F-FUdR was prepared using automated radiofluorodestannylation of Bu_3SnUdR-$(OAc)_2$. The radiofluorinating agent ^{18}F-F_2 was produced via ^{10}Ne(d,α)^{18}F nuclear reaction. About 5.55 Bq (~150 mCi) ^{18}F-F_2 were produced with an 8.5-MeV deuteron irradiation (60 μA·h current integration) of Ne mixed with 200 μmol of carrier F_2. ^{18}F-F_2 produced from the cyclotron was bubbled (200 mL/min) into a precooled solution of

$Bu_3SnUdR\text{-}(OAc)_2$ (50 mg, 83.2 mmol) in Freon-11 (18 mL, Merck) at ambient temperature over a period of 14 min. The solvent was evaporated at 50°C with a gentle stream of nitrogen. The residue was dissolved in methylene chloride (15 mL) and then transferred to a silica gel column (1.0-cm inner diameter, 2.0 g) and a sodium thiosulfate column (0.6-cm inner diameter, 0.3 g). The columns were eluted with 15 mL of ether. The eluate was evaporated under a gentle stream of nitrogen at 80°C. The residue was then hydrolyzed with 1 mL of 0.5N NaOH at 90°C for 5 min. After cooling to room temperature, the reaction mixture was neutralized with 1 mL of 0.5N HCl, filtered with a 0.22-μm membrane disk, and subjected to semipreparative radio–high-performance liquid chromatographic (HPLC) separation (Econosil C-18; 10 μm, 10×250 mm column; eluent, 3% ethanol in water; flow rate, 1 mL/min; radiodetector, Flow Count FC-004; Bioscan) to afford the ^{18}F-FUdR product (retention time = 9.5 to ~10 min). The specific activity was determined with the radio-HPLC calibration curve. Thin-layer chromatography (TLC) was performed on a silica gel aluminum sheet using ethyl acetate/ethanol = 90:10 (v/v) as the developing agent. The R_f of ^{18}F-FUdR was 0.52. Both the HPLC and the TLC analysis of ^{18}F-FUdR were consistent with that of authentic FUdR standard purchased from Merck. The ^{1}H NMR spectrum of ^{18}F-FUdR—determined at 24 h after preparation, allowing ^{18}F to decay—was also in agreement with the FUdR standard.

The radiochemical purity of ^{18}F-FUdR was >98% with 1.66×10^6 MBq/mmol of specific activity. The radiochemical yield (end of bombardment) was about 30%–50% based on the radioactivity of $^{18}F\text{-}F_2$ and the overall yield was about 52%. Both the radiolabeling yield and the radiochemical yield in ^{18}F-FUdR preparation by radiofluorodestannylation from the organotin precursors were significantly improved over those produced by direct radiofluorination of deoxyuridine (*30–34*).

Synthesis of ^{18}F-FET

^{18}F-FET was synthesized as described (*27–29*) with minor modifications. Briefly, ^{18}F-fluoride in tetra-*n*-butyl ammonium (TBA) bicarbonate (TBA ^{18}F-fluoride) and *N*-BOC-(*O*-(2-tosyloxyethyl)-L-Tyr-Obz (5 mg, 9.35 μmol) were mixed with 0.8 mL of anhydrous acetonitrile in the reaction vial. The mixture was heated at 90°C for 10 min. Thereafter, the solution was evaporated to dryness under reduced pressure. After cooling to room temperature, the residue was dissolved in 1.5 mL of methylene chloride. The solution was loaded into a chromatography column (silica gel, 1.0 g) and eluted with 2.5 mL of diethyl ether. The eluate was evaporated to dryness under a gentle stream of helium at 50°C. The residue was dissolved in 0.3 mL ethanol and hydrolyzed with 0.3 mL of 1N HCl at 100°C for 10 min. The reaction mixture was neutralized with 0.3 mL of 1N NaOH and 1.4 mL distilled water. The solution was filtered through a 0.22-μm membrane to give the isotonic L-^{18}F-FET product. The radiochemical purity of L-^{18}F-FET was determined using radio-TLC. Radio-TLC was performed on an aluminum sheet coated with silica gel powder using 10 mmol/L ammonium acetate/acetonitrile = 30:70 (v/v) as the developing agent. The radiochemical yield was about 55% and the radiochemical purity was >98%.

Synthesis of ^{123}I-FIAU

^{123}I-FIAU was synthesized from 5-tributylstannyl-2′-fluoro-1-β-D-arabino-furanosyluracil (FTAU), as described (*12–14*). The radiochemical purity of ^{123}I-FIAU was determined using radio-TLC. Radio-TLC was performed on the aluminum sheet coated with silica gel powder (Silica gel 60, 70-230 mesh; Merck) by using ethyl acetate/ethanol = 90:10 (v/v) as the mobile phase. The final product, lyophilized ^{123}I-FIAU, was redissolved in ethanol and the radiochemical purity was determined using radio-TLC, which showed the R_f of ^{123}I-FIAU to be 0.82–0.83, which was the same as that obtained from an authentic FIAU standard. The labeling yield was >95% and the radiochemical purity was >98%.

Synthesis of ^{18}F-FDG

^{18}F-FDG was prepared according to Lemaire et al. (*35*) using an automated ^{18}F-FDG synthesis system (Coincidence Technologies) at the National PET/Cyclotron Center in Taipei.

Cell Cultures

NG4TL4 sarcoma cells were cultured in MEM supplemented with 10% FBS in a humidified atmosphere with 5% CO_2 at 37°C. *HSV1-tk*–positive NG4TL4 cells (NG4TL4-STK) were generated by transfection of NG4TL4 cells with a conditioned medium from the PA317-tk retroviral vector producer cells, which produce replication-incompetent retroviruses carrying *HSV1-tk* and *NeoR* genes. A stably transduced population of NG4TL4-STK cells was obtained by selection in medium supplemented with G418 (1 mg/mL).

In Vitro Accumulation of ^{123}I-FIAU, ^{18}F-FUdR, ^{18}F-FET, and ^{18}F-FDG

One million NG4TL4 cells or NG4TL4-STK cells were seeded into 6-well culture plates containing 2 mL of MEM supplemented with 10% FBS. After 24 h of growth, 100-μL aliquots of ^{123}I-FIAU, ^{18}F-FUdR, or ^{18}F-FDG (3.7 MBq/mL) were added to the cell culture medium. After 4 h of tracer incubation, the culture medium was removed and the monolayers were washed 3 times with 2 mL of cold PBS. The cells were harvested from the culture plates by treatment with 0.1 mL of 0.5% trypsin for 5 min. The cells were resuspended in 2 mL of culture medium to neutralize the trypsin. A 50-μL sample was taken to assess cell viability with trypan blue and count the number of viable cells under a microscope. The radioactivity concentration in the cell suspensions was measured in a γ-counter (Cobra II; Packard Instruments) and normalized to the number of viable cells in the cell suspensions. The accumulation of radiotracers was expressed as the percentage of the tracer dose added to the medium that had accumulated in 1 million cells (% dose/10^6 cells).

In Vitro ^{123}I-FIAU Accumulation of Cells with Various Percentages of HSV1-tk–Expressing Cells

One million NG4TL4 cells, NG4TL4-STK cells, or mixtures of NG4TL4 cells and different percentages of NG4TL4-STK cells were seeded in 6-well culture plates. After 24 h at 37°C, 100-μL aliquots of ^{123}I-FIAU (3.7 MBq/mL) were added to the medium in each well. The radioactivity concentration in the cell suspensions was measured as described.

Tumor Xenografts in Mice

The experimental protocol was approved by the Institutional Animal Care and Use Committee of the National Yang-Ming University (Taipei, Taiwan). Multiple subcutaneous xenografts of different tumors were produced in FVB/N female mice under anesthesia (ketamine [87 mg/kg] and xylazine [13 mg/kg], intraperitoneally). Each tumor xenograft was produced by subcutaneous injection of a mixture of NG4TL4 cells with different percentages of NG4TL4STK-positive cells (total, 1×10^6 cells in 0.2 mL of Hanks' balanced salt solution). The location of

tumors was as follows: (a) left shoulder, 100% NG4TL4-STK + 0% NG4TL4; (b) left thigh, 50% NG4TL4-STK + 50% NG4TL4; (c) right thigh, 25% NG4TL4-STK + 75% NG4TL4; and (d) right shoulder, 0% NG4TL4-STK + 100% NG4TL4. Studies were conducted when the tumors were 0.8–1.0 cm in diameter. Sixty-eight animals were used in these studies: 60 mice were used for tumor burden determination and, of these, 36 were used for biodistribution studies (3 mice per tracer per time point). Eight mice were used in microPET/scintigraphic imaging (2 mice per tracer). GCV was administered in the therapeutic group as daily 10 mg/kg intraperitoneal injections. After an imaging study, the tumors were excised and then weighted. The average weights of the tumors established from the NG4TL4 cells mixed with 0%, 25%, 50%, or 100% NG4TL4-STK cells were 0.21 ± 0.10, 0.29 ± 0.22, 0.16 ± 0.06, and 0.24 ± 0.13 g, respectively ($n = 5$).

microPET/Planar γ-Imaging Studies

Imaging studies were performed 1 d before and at 4 d and 7 d of GCV therapy. The mice were anesthetized with 0.1% isofluorane in oxygen. Planar γ-imaging was performed using a dual-head γ-camera (ECAM; Siemens) equipped with a pinhole collimator. A static emission scan was acquired for 20 min at 24 h after intravenous administration of 7.4 ± 0.1 MBq of ^{123}I-FIAU.

PET was performed on a microPET R4 scanner (Concorde Microsystems, Inc.). The scanner has a computer-controlled bed and 10.8-cm transaxial and 8-cm axial field of view. It has no septa and operates exclusively in 3-dimensional list mode. All raw data were first sorted into 3-dimensional sinograms, followed by Fourier rebinning and ordered-subsets expectation maximization image reconstruction. Fully 3-dimensional list-mode data were collected using an energy window of 350–750 keV and a time window of 6 ns. Image pixel size was 0.85 mm transaxially with a 1.21-mm slice thickness. Static imaging was performed with 3 groups of mice (2 mice per group) for 20 min at 4, 1, or 1 h after intravenous injection of 3.7 ± 0.2 MBq of ^{18}F-FUdR, ^{18}F-FET, or ^{18}F-FDG, respectively. The tumor-bearing mice were positioned in the microPET camera with their long axis parallel to the transaxial plane of the tomography and placed near the center of the field of view of the microPET, where the highest image resolution and sensitivity are available.

To estimate radioactivity concentration, regions of interest were drawn over the target tumors and tissues (i.e., muscle) and the values were corrected by subtracting background levels of radioactivity, which was measured in the remote areas away from the animal body. Tumor radioactivity concentration was normalized by that in the muscle and expressed as the tumor-to-muscle accumulation ratio.

Tissue Sampling and Radioactivity Measurements

The mice were sacrificed by cervical dislocation at 24, 4, 1 h before, or 1 h after ^{123}I-FIAU, ^{18}F-FUdR, ^{18}F-FET, or ^{18}F-FDG injection, respectively. Tumors and 10 other tissues (blood, heart, lung, liver, stomach, small intestine, large intestine, spleen, kidney, and muscle) were dissected, washed, and weighted. The radioactivity concentration in these tissue samples was measured by γ-spectrometry (Cobra II), normalized to sample weight, and expressed as the percentage of injected dose per gram of tissue (%ID/g) and the tumor-to-blood accumulation ratio.

Statistical Analysis

The statistical significance of comparisons of tumor weight and tumor tracer uptake between groups of mice was based on 2-sided, 2-sample Student t tests. Values of $P < 0.05$ were considered statistically significant. Results are reported as mean ± SD. Linear and nonlinear regression was used to analyze the relationship between the number of *HSV1-tk*–positive cells and the level of ^{123}I-FIAU accumulation in tumors as well as the relationship between the number of *HSV1-tk*–positive cells and the magnitude of decrease in accumulation of each imaging agent induced by therapy with GCV.

RESULTS

In Vitro ^{123}I-FIAU, ^{18}F-FUdR, ^{18}F-FET, and ^{18}F-FDG Accumulation

The ^{123}I-FIAU accumulation in NG4TL4-STK cells increased linearly with time (Fig. 1A), whereas almost no accumulation of ^{123}I-FIAU was observed in NG4TL4 cells. The ^{18}F-FUdR accumulation in both NG4TL4 and NG4TL4-STK cells reached a maximum at 30 min and then declined slowly with time; the level of accumulation of ^{18}F-FUdR in NG4TL4-STK cells was higher than that in the wild-type NG4TL4 cells (Fig. 1B). The ^{18}F-FDG accumulation in both NG4TL4 and NG4TL4-STK cells increased linearly with time, and the NG4TL4 cells showed higher uptake levels (Fig. 1C). The accumulation of L-^{18}F-FET in vitro at 4 h of incubation was slightly higher in NG4TL4-STK cells than that in NG4TL4 cells (Fig. 1D).

In Vitro ^{123}I-FIAU Accumulation of Cells with Various Percentages of HSV1-tk–Expressing Cells

To determine whether the level of ^{123}I-FIAU accumulation correlated with the level of *HSV1-tk* gene expression in the transduced cell population, radiotracer accumulation

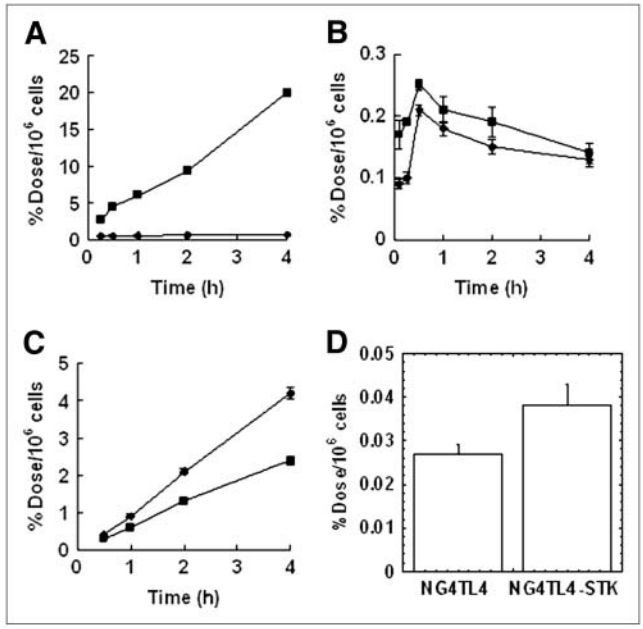

FIGURE 1. Accumulation of ^{123}I-FIAU (A), ^{18}F-FUdR (B), and ^{18}F-FDG (C) in NG4TL4 cells (◆) and NG4TL4-STK cells (■) up to 4 h of incubation. (D) Accumulation of ^{18}F-FET at 4 h of incubation. Uptake was expressed as %ID/10^6 cells. Values in B and D are shown as mean ± SD.

assays were performed, in which the HSV-TK–positive and wild-type tumor cells were mixed at varying ratios. After a 4-h incubation period, up to 5.44% ± 0.18% of ^{123}I-FIAU had accumulated per million NG4TL4-STK cells, whereas only negligible low uptake was found in NG4TL4 control cells (0.42% ± 0.03% dose per 10^6 cells). A linear correlation was observed between the ^{123}I-FIAU accumulation and the percentage of NG4TL4-STK cells mixed with the population of wild-type cells ($r^2 = 0.98$; Fig. 2A).

Effect of GCV Therapy on Tumor Size

One day before GCV treatment, the weights of tumors with different percentages of NG4TL4-STK and wild-type NG4TL4 cells were similar (Table 1). After GCV treatment, the weights of tumors containing different percentages of NG4TL4-STK cells showed no significant changes compared with the corresponding pretreatment weights. In contrast, the weights of NG4TL4 tumors (0% NG4TL4-STK cells) increased significantly despite GCV treatment ($P < 0.001$).

microPET/Planar γ-Imaging with ^{123}I-FIAU, ^{18}F-FUdR, ^{18}F-FDG, and ^{18}F-FET

High levels of ^{123}I-FIAU radioactivity accumulation and high tumor-to-blood ratios in NG4TL4-STK tumors revealed a high level of *HSV1-tk* expression. In contrast, in wild-type tumors, the level of ^{123}I-FIAU radioactivity accumulation did not differ from the body background level (Fig. 3A). After 4 and 7 d of GCV treatment, γ-camera imaging revealed significantly reduced levels of ^{123}I-FIAU accumulation within all NG4TL4-STK cell–containing tumors. This indicated that most of tumor cells expressing the *HSV1-tk* gene were killed by GCV after 4 d of treatment.

In parallel, microPET with ^{18}F-FUdR revealed significant inhibition of nucleotide use and proliferative activity in all NG4TL4-STK cell–containing tumors (Fig. 3B). In contrast, no significant differences in ^{18}F-FDG accumulation were observed throughout GCV therapy within all tumors (Fig. 3C). Marked inhibition of ^{18}F-FET accumulation was observed in tumors composed of 100% NG4TL4-STK cells after 7 d of GCV therapy (Fig. 3D), whereas tumors with lower percentages of NG4TL4-STK cells demonstrated only small changes or no changes in ^{18}F-FET accumulation during the course of GCV therapy.

Quantitation of ^{123}I-FIAU, ^{18}F-FUdR, ^{18}F-FET, and ^{18}F-FDG in Tumors Measured by Tissue Sampling

^{123}I-FIAU accumulation in tumors before GCV therapy exhibited a strong logarithmic–linear relationship with the percentage of NG4TL4-STK cells in tumors ($r^2 = 0.96$; Fig. 2B). After 4 and 7 d of GCV treatment, all *HSV1-tk*–expressing tumors exhibited a significant decrease in ^{123}I-FIAU accumulation ($P < 0.005$) compared with that of nontreated controls (Figs. 4A and 4E). These findings demonstrate that most of tumor cells expressing the *HSV1-tk* gene were eliminated by therapy with GCV. In contrast, no differences in ^{123}I-FIAU accumulation (which was very low) were observed between GCV-treated and control groups of animals bearing tumors that developed only from the wild-type NG4TL4 cells (Figs. 4A and 4E).

^{18}F-FUdR accumulation in all *HSV1-tk*–expressing tumors was very similar before GCV therapy, decreased significantly at day 4 of GCV therapy ($P < 0.005$), and had a tendency to decrease slightly further at day 7 of GCV therapy ($P < 0.005$) compared with pretreatment levels (Figs. 4B and 4F). The overall magnitude of decrease in ^{18}F-FUdR accumulation was independent of the percentage of *HSV1-tk*–expressing cells, at least down to 25% of *HSV1-tk*–expressing cells in tumors. Analysis of the tumor-to-blood ratios demonstrated a more significant decrease in ^{18}F-FUdR accumulation in tumors with a higher percentage of *HSV1-tk*–expressing cells (Fig. 4F).

In NG4TL4 tumors, no statistically significant differences in ^{18}F-FUdR accumulation were observed between GCV-treated and nontreated groups.

^{18}F-FDG accumulation in all tumors before therapy was statistically similar but demonstrated a trend to decrease during the course of GCV therapy in *HSV1-tk*–expressing tumors (Figs. 4C and 4G). A statistically significant decrease in ^{18}F-FDG accumulation was observed only at day 7 of GCV therapy compared with pretreatment levels ($P < 0.05$). The magnitude of decrease in ^{18}F-FDG accumulation was independent of the percentage of *HSV1-tk*–expressing

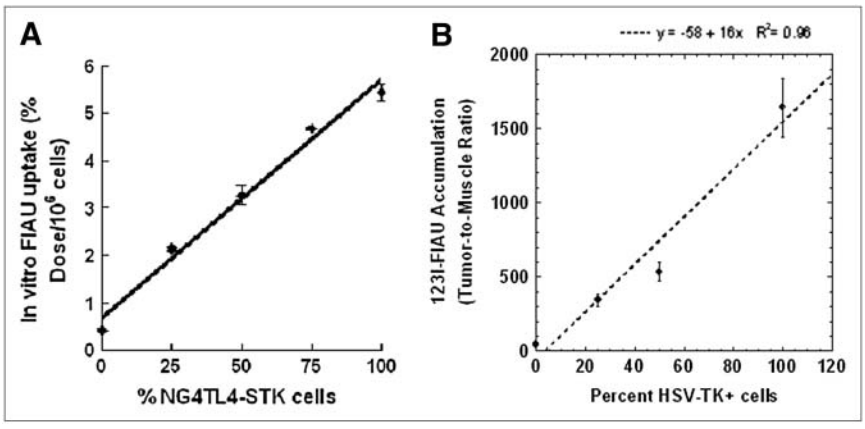

FIGURE 2. Level of *HSV1-tk* gene expression in cell cultures and in tumors with different percentage of NG4TL4-STK cells. (A) Cellular ^{123}I-FIAU accumulation vs. fraction of NG4TL4-STK cells ($r^2 = 0.98$). (B) Relationship between in vivo tumor ^{123}I-FIAU uptake (tumor-to-muscle ratio) vs. percentage of *HSV1-tk*–expressing cells in tumor.

TABLE 1
Tumor Burden of FVB/N Female Mice Before and During GCV Consecutive Treatment

NG4TL4-STK (%)	Tumor burden (g)		
	Day 0	Day 4*	Day 7*
100†	0.24 ± 0.13‡	0.19 ± 0.09§‖	0.10 ± 0.06§‖
50†	0.16 ± 0.06‡	0.23 ± 0.14§‖	0.19 ± 0.07§‖
25†	0.29 ± 0.22‡	0.21 ± 0.07§‖	0.31 ± 0.22§‖
0	0.21 ± 0.10	1.08 ± 0.25¶	1.81 ± 0.54¶

*Compared with day 0 by *t* test.
†Compared with 0% tk tumor by *t* test.
‡*P* = not significant when compared with 0% tk tumor.
§*P* < 0.001 when compared with 0% tk tumor.
‖*P* = not significant when compared with day 0.
¶*P* < 0.001 when compared with day 0.
Data are expressed as mean ± SD.

cells, at least down to 25% of *HSV1-tk*–expressing cells in tumors (Fig. 4C). However, tumor-to-blood ratios of ^{18}F-FDG accumulation decreased more in tumors with higher percentages of *HSV1-tk*–expressing cells (Fig. 4G). In NG4TL4 tumors, no statistically significant differences in ^{18}F-FDG accumulation were observed between GCV-treated and nontreated groups.

^{18}F-FET accumulation in all tumors before therapy was statistically similar (Figs. 4D and 4H). Although a moderate decrease in ^{18}F-FET accumulation levels was observed in all tumors after 4 d of GCV therapy, there were no differences in tumor-to-blood ratios of ^{18}F-FET accumulation (Figs. 4D and 4H). Only after 7 d of GCV therapy was a trend toward lower tumor-to-blood ratios of ^{18}F-FET accumulation observed in tumors with a higher percentage of *HSV1-tk*–expressing cells (Fig. 4H).

Relationships Between Initial ^{123}I-FIAU Accumulation and Changes in ^{18}F-FUdR, ^{18}F-FDG, and ^{18}F-FET Accumulation During GCV Therapy

As described earlier, the ^{123}I-FIAU accumulation in tumors (expressed as the tumor-to-muscle accumulation ratio) was strongly related to the percentage of *HSV1-tk*–expressing cells in tumors and may be used as a noninvasive measure of the level of *HSV1-tk* expression in tumors. Next, we analyzed the relationships between the level of ^{123}I-FIAU accumulation in tumors and the magnitude of decrease (fold decrease) in the accumulation of ^{18}F-FUdR, ^{18}F-FDG, and ^{18}F-FET in tumors in response to GCV therapy.

The strongest relationship was observed between the pretreatment levels of ^{123}I-FIAU accumulation and the fold decrease in ^{123}I-FIAU accumulation after 4 d and, especially, after 7 d of GCV therapy (Fig. 5A). Also, a strong relationship was observed between the fold decrease in ^{18}F-FUdR accumulation at 4 and 7 d of GCV treatment and the pretreatment levels of ^{123}I-FIAU accumulation (Fig. 5B). In contrast, no relationship was observed at 4 d of GCV therapy between the fold decrease in ^{18}F-FDG and ^{18}F-FET accumulation and the pretreatment levels of ^{123}I-FIAU accumulation in tumors (Figs. 5C and 5D). After 7 d of GCV therapy, a strong relationship was observed between the fold decrease in ^{18}F-FDG and ^{18}F-FET accumulation and the pretreatment levels of ^{123}I-FIAU accumulation (Figs. 5C and 5D). However, the magnitudes of changes (fold decrease) in accumulation of both ^{18}F-FDG and ^{18}F-FET as a function of pretreatment levels of ^{123}I-FIAU accumulation were very small (1.1- to 2.1-fold) compared with that for ^{18}F-FUdR accumulation (2- to 10-fold).

DISCUSSION

For more than a decade, gene therapy with the *HSV1-tk* suicide gene in combination with the prodrug GCV was explored as a treatment modality for cancer (*1–5*). After GCV is phosphorylated by the HSV1-TK to GCV monophosphate, it is phosphorylated further to GCV di- and triphosphate by endogenous cellular kinases and incorporated into proliferating tumor cell DNA, which causes DNA chain termination and induces tumor cell apoptosis. The major obstacle for wide clinical application of this approach remains the insufficient amounts of the suicide gene delivered into the target tumor tissue. To eliminate this obstacle, more than a decade ago, in 1995, Tjuvajev et al. (*36*) developed an approach for noninvasive imaging of the location, magnitude, and persistence of *HSV1-tk* gene expression in tumors. Nevertheless, the clinical translation of this technology has been slow, and only a few clinical gene therapy trials have used PET for monitoring the *HSV1-tk* expression levels in tumors (*15,16*). To our knowledge, the first-ever clinical study was reported by Jacobs et al. (*15*) in 2001, in which PET with ^{124}I-FIAU at 72 h after injection of the tracer revealed specific accumulation and retention sites in tumor tissue in 1 patient with a glioblastoma lesion that had been transfected with *HSV1-tk* using a liposomal vector. However, no specific accumulation and retention of the tracer in the lesions of 4 other treated patients was observed, and issues related to the blood–brain barrier have been raised in this study. In 2005, Panuelas et al. (*16*) reported that transgene expression monitoring by ^{18}F-FHBG PET performed just 2 d after injection of a gene delivery vector (and before starting the GCV treatment) could be used to predict the response to the gene therapy procedure in cancer patients. This study demonstrated stabilization of disease, when evaluated 30 d after the gene therapy procedure, only in those patients in whom the ^{18}F-FHBG accumulation was observed in the treated nodules. In contrast, those patients with ^{18}F-FHBG PET–negative tumor nodes exhibited a progression of the disease.

In the current study we modeled different levels and distributions of *HSV1-tk* expression within tumors by mixing *HSV1-tk*–expressing sarcoma cells with wild-type sarcoma cells (0%, 25%, 50%, and 100%) when establishing tumor xenografts in mice. Using this model we demonstrated that

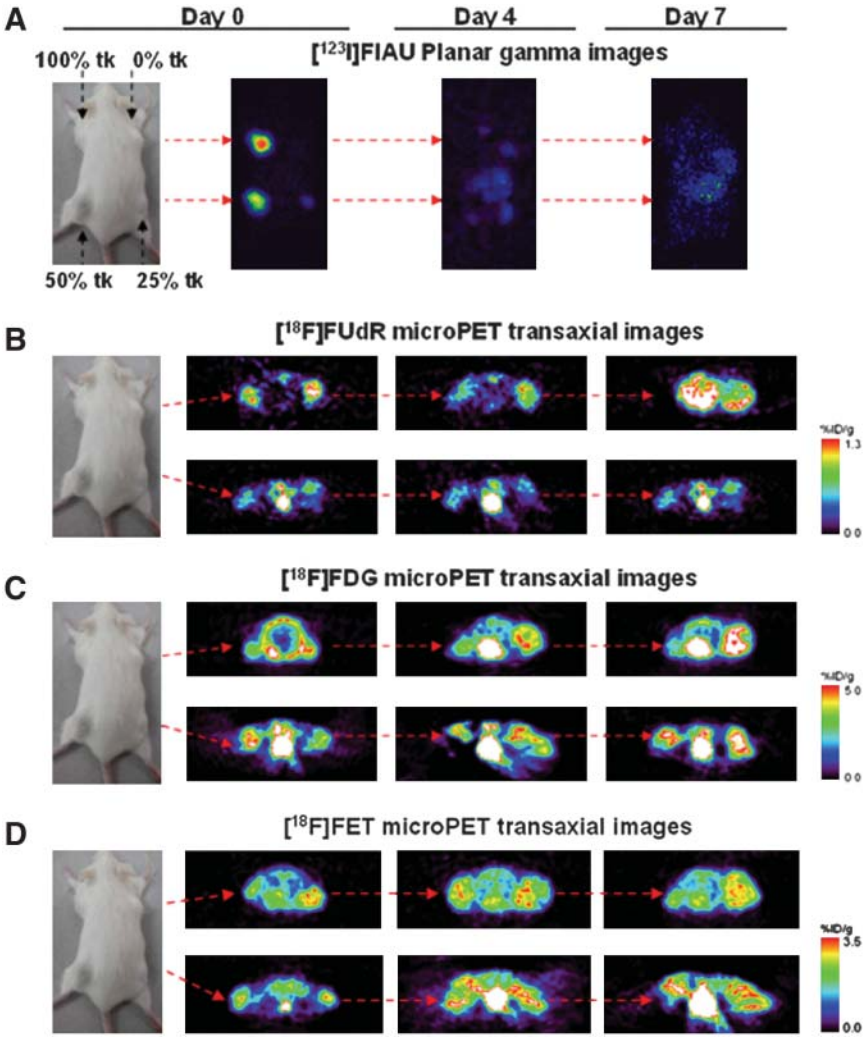

FIGURE 3. Representative microPET/planar γ-images of tumor-bearing FVB/N mice after injection of ^{123}I-FIAU (A), ^{18}F-FUdR (B), ^{18}F-FDG (C), and ^{18}F-FET (D). Imaging time for ^{123}I-FIAU, ^{18}F-FUdR, ^{18}F-FDG, and ^{18}F-FET was 24, 4, 1, and 1 h, respectively.

the level of ^{123}I-FIAU accumulation expressed as the tumor-to-muscle ratio in tumors is strongly related to the percentage of *HSV1-tk*–expressing cells (Fig. 2B). This observation is supported by a previously published study, which showed that ^{124}I-FIAU PET was able to distinguish different levels of *HSV1-tk* expression in tumor xenografts grown in rats from single-cell–derived clones of tumor cells expressing different levels of *HSV1-tk* gene (*6*). We also demonstrated that the level of ^{123}I-FIAU accumulation is strongly predictive of tumor responses to GCV therapy (Table 1; Figs. 3A, 4A, and 5A) and that the magnitude of decrease in ^{123}I-FIAU accumulation during GCV therapy is strongly related to the percentage of *HSV1-tk*–expressing cells in tumors. These observations are in agreement with a previous report, which showed that the KBALB-STK tumors expressing *HSV1-tk* could be readily detected with γ-camera imaging using another *HSV1-tk*–specific pyrimidine nucleoside analog, (*E*)-5-(2-^{131}I-iodovinyl)-2′-fluoro-2′-deoxyuridine (^{131}I-IVFRU), and that a single dose of GCV (100 mg/kg intraperitoneally) significantly decreased tumor uptake of ^{131}I-IVFRU (*37*). Subsequent single daily doses of GCV over 3 consecutive days had a negligible effect on ^{131}I-IVFRU uptake, which remained low. Our observations are also supported by a recently reported clinical study, which demonstrated that only those tumors accumulating ^{18}F-FHBG regressed after GCV treatment (*19*). This study also showed that ^{18}F-FHBG (%ID) declines during GCV therapy and that ^{18}F-FHBG PET can be used to monitor the effectiveness of GCV treatment.

Another impediment to clinical translation of prodrug activation gene therapy protocols is the lack of information relating to the feasibility of monitoring the early responses to such therapies with clinically applicable molecular imaging agents, such as ^{18}F-FDG. Changes in tumor glucose metabolism, protein synthesis, and cell proliferation induced in the gene-transduced cells and surrounding nontransduced cells may be indicative of early responses to therapy and should be explored in a rigorous manner.

For this purpose, in the current study we assessed the efficacy of 3 radiotracers—^{18}F-FUdR, ^{18}F-FDG, and ^{18}F-FET—that are used for imaging of tumor proliferation (nucleic acid synthesis), glucose metabolism (viability), and amino acid transport (protein synthesis), respectively, for their potential in monitoring tumor responses of *HSV1-tk*

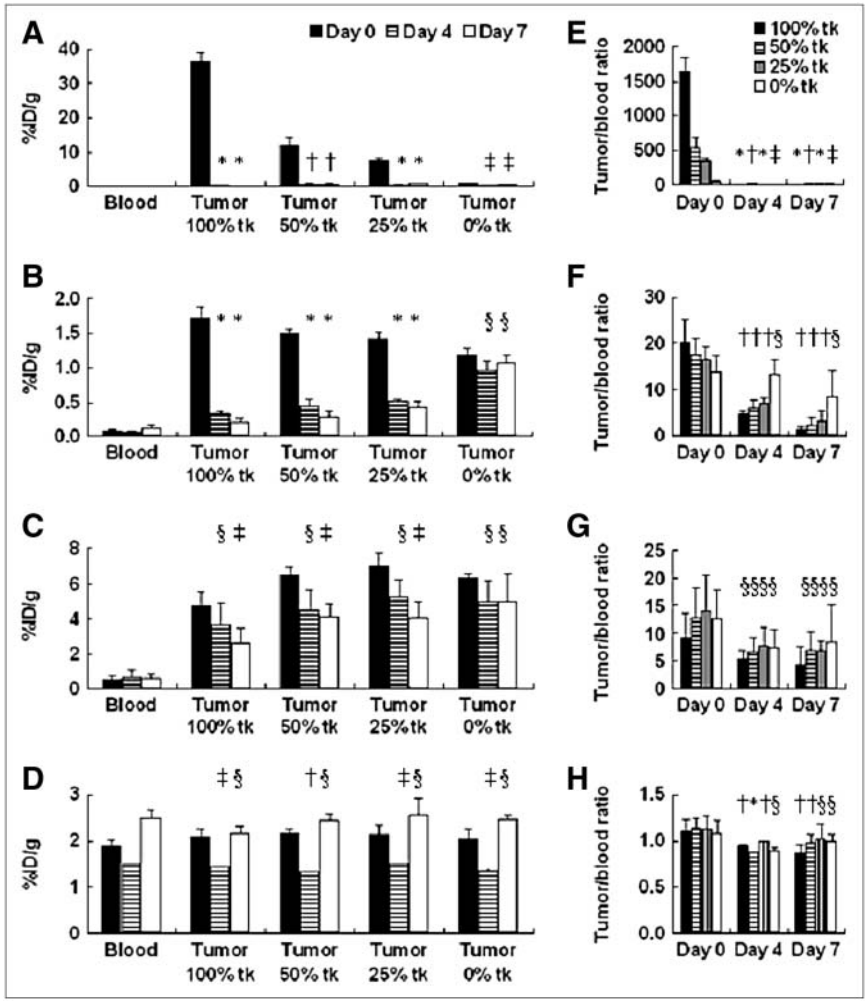

FIGURE 4. Radioactivity in tumors and blood (%ID/g) and tumor-to-blood ratios in tumor xenografts with different percentages of *HSV1-tk*–expressing cells after intravenous injection in mice with ^{123}I-FIAU (A and E), ^{18}F-FUdR (B and F), ^{18}F-FDG (C and G), and ^{18}F-FET (D and H) before GCV therapy and after 4 and 7 d of treatment. For each group of tumors, uptake values on day 4 and day 7 were compared with that on day 0. $^{*}P < 0.0002$; $^{\dagger}P < 0.005$; $^{\ddagger}P < 0.05$; and $^{\S}P$ = not significant.

suicide gene therapy. To evaluate responses to GCV therapy as a function of *HSV1-tk* gene expression levels, we used a multitumor model, in which 4 tumors with different percentages of *HSV1-tk*–expressing sarcoma cells (0%, 25%, 50%, and 100%) were grown in the same animal to facilitate comparisons between tumors and different radiotracers before and during the course of GCV therapy. Using dynamic PET and analysis of radiotracer accumulation in tissue samples obtained from tumors and nontumor tissues, we show that PET with ^{18}F-FUdR is applicable for monitoring changes in tumor proliferation during *HSV1-tk* and GCV prodrug activation gene therapy, because of a strong relationship that was observed between the fold decrease in ^{18}F-FUdR accumulation at 4 and 7 d of GCV treatment and pretreatment levels of ^{123}I-FIAU accumulation (Fig. 5B), which reflects the level of *HSV1-tk* gene expression in tumors. Our findings using repetitive ^{18}F-FUdR PET are in agreement with a previous report that showed that 4 d of GCV therapy (100 mg/kg) inhibited proliferative activity and ^{3}H-thymidine incorporation into DNA of *HSV1-tk*–expressing GCV-treated subcutaneous Morris hepatomas down to 10.5% of the nontreated controls (*17*). In contrast, in our sarcoma subcutaneous tumor model, no relationship was observed at 4 d of GCV therapy between the magnitude of decrease (fold decrease) in ^{18}F-FDG accumulation and pretreatment levels of ^{123}I-FIAU accumulation in tumors. Only at 7 d of GCV therapy was a strong relationship observed between the magnitude of decrease in ^{18}F-FDG accumulation and pretreatment levels of ^{123}I-FIAU accumulation. However, the magnitudes of decrease in accumulation of ^{18}F-FDG as a function of pretreatment levels of ^{123}I-FIAU accumulation were very small (1.5- to 2.1-fold) compared with that for ^{18}F-FUdR accumulation (2- to 10-fold). One explanation for the lack of changes in ^{18}F-FDG accumulation even in tumors consisting of 100% *HSV1-tk*–expressing cells is that in this sarcoma model the ^{18}F-FDG accumulation can be due to the inflammatory-related cells, such as macrophages, as previously reported for other tumors (*8*). Our current results are also in agreement with several other previously reported studies. For example, in intracerebral RG2TK-positive gliomas in rats it was shown that 3 d of GCV (50 mg/kg intraperitoneally twice a day) had only a small, albeit statistically significant, effect on glucose use (*18*). In another study, dynamic PET measurements of ^{18}F-FDG uptake were performed on animals bearing subcutaneous *HSV1-tk*–expressing and wild-type Morris hepatomas

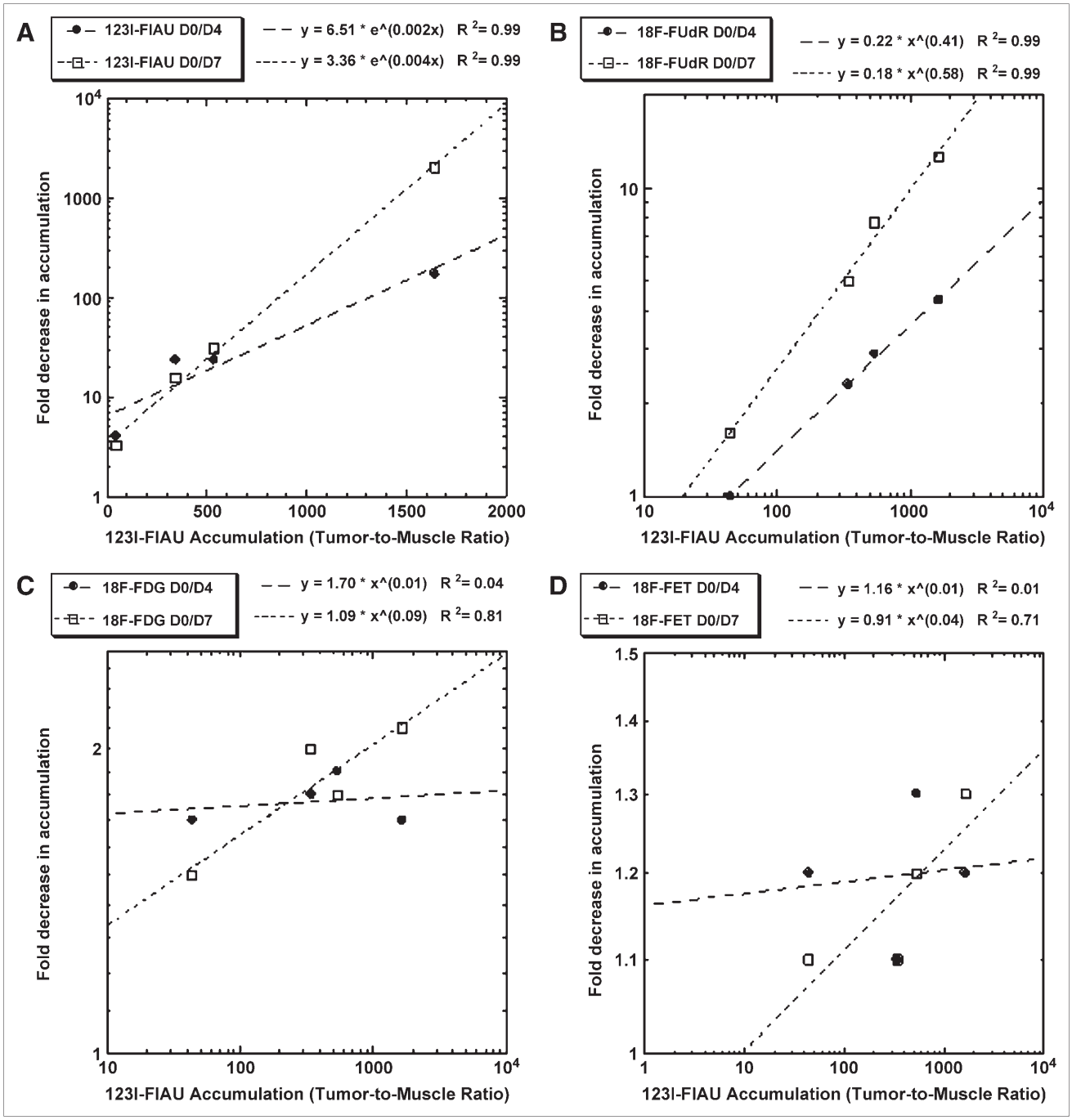

FIGURE 5. Relationships between pretreatment levels of ^{123}I-FIAU accumulation before therapy in tumors with different percentages of *HSV1-tk*–expressing cells and corresponding decreases in accumulation of ^{123}I-FIAU (A), ^{18}F-FUdR (B), ^{18}F-FDG (C), and ^{18}F-FET (D) after 4 and 7 d of therapy with GCV uptake before treatment. Each point represents the average ratio of day 0/day 4 or day 0/day 7 (fold decrease) in radiotracer accumulation in tumors with different percentages of *HSV1-tk*–expressing cells. Dotted and dashed lines and equations demonstrate results of regression analyses.

at 2 and 4 d after the onset of therapy with GCV (100 mg/kg) (*17*). An uncoupling of ^{18}F-FDG transport and phosphorylation was found with enhanced k_1 and k_2 values and a normal k_3 value after 2 d of GCV treatment. The increase in ^{18}F-FDG transport normalized after 4 d compared with pretreatment levels, whereas the phosphorylation rate, k_3, increased.

In yet another study, the effect of acyclovir (ACV) on the metabolism of rat 9L gliosarcoma cells expressing the herpes simplex virus thymidine kinase gene was studied using ^{18}F-FDG and L-[methyl-^{11}C]methionine. Though the average weight of the tumors treated with ACV was significantly lower than that of the saline-injected control group,

^{18}F-FDG and ^{11}C-methionine uptake per weight of tumor tissue did not differ between the 2 groups (*21*).

A possible underlying mechanism for these observations and our findings is that a redistribution of the glucose transport protein from intracellular pools to the plasma membrane may be considered and is observed in cell culture studies as a general reaction to cellular stress (*38*).

In general, GCV is thought to increase glucose transport and utilization (*38*) and decrease amino acid transport (*39*). In previous in vitro studies, Haberkorn et al. found a decrease in aminoisobutyric acid and methionine uptake in vitro in LXSNtk8 cells after GCV treatment and concluded that neutral amino acid transport and protein synthesis in the tumor cells were impaired after gene therapy with the HSVtk/GCV suicide system (*39*).

Our current studies demonstrated that, after 4 d of GCV therapy, the ^{18}F-FET tumor-to-blood and tumor-to-muscle ratios did not decrease substantially compared with pretreatment levels in tumors with different percentages of *HSV1-tk*–expressing cells. Only after 7 d of GCV therapy was a strong relationship observed between the fold decrease in ^{18}F-FET accumulation and pretreatment levels of ^{123}I-FIAU accumulation. However, the magnitudes of change (fold decrease) in accumulation of ^{18}F-FET as a function of pretreatment levels of ^{123}I-FIAU accumulation were very small (1.1- to 1.3-fold) compared with that for ^{18}F-FUdR accumulation (2- to 10-fold). The observed decrease in ^{18}F-FET accumulation was less substantial in the our studies. For example, GCV treatment reduced the partial differential K_1 and the % dose/g of ^{14}C-aminocyclopentane carboxylic acid (^{14}C-ACPC) in RG2TK-positive xenografts to approximately 30% of that in nontreated animals (*18*). These differences may be due to the levels of L-amino acid transporter expression and proliferative activity in different tumor models, which determines the additional sensitivity to GCV.

Therefore, in a future clinical scenario, the adequacy of distribution and magnitude of *HSV1-tk* gene expression before initiation of GCV therapy should be assessed initially with ^{124}I-FIAU PET/CT or another suitable HSV1-tk–specific tracer (^{18}F-FEAU, ^{18}F-FHBG, and so forth), and the baseline nucleoside metabolism and proliferative activity can be assessed with ^{18}F-FUdR (or ^{18}F-FLT); then, therapy with GCV could be initiated and its efficacy could be assessed early by repetitive PET/CT with ^{18}F-FUdR (or ^{18}F-FLT).

The implementation of noninvasive imaging technologies for the assessment of *HSV1-tk* gene expression in future clinical gene therapy protocols should allow avoidance of suboptimal prodrug activation treatments—gene therapy may be optimized with respect to vector dose or GCV dose and time after vector administration—to ensure the maximum transgene expression and the maximum therapeutic effect. Furthermore, when using prodrugs such as GCV, tumor responses (metabolic, proliferative, and so forth) could be serially monitored, with the dosing or the duration of treatment modified as necessary, to achieve the maximum therapeutic effect. Alternatively, patients could be switched to other treatment regimens at a very early stage.

CONCLUSION

We have evaluated the efficacy of multimodality imaging with 4 different radiotracers—^{123}I-FIAU, ^{18}F-FUdR, ^{18}F-FDG, and ^{18}F-FET—for the prediction and monitoring of early responses in tumors to prodrug activation gene therapy with *HSV1-tk* and GCV. γ-Camera imaging with ^{123}I-FIAU is a reliable method for detection of the location and magnitude of *HSV1-tk* expression in gene-targeted tumors and for prediction of the sensitivity of transfected tumor tissue to therapy with GCV. Repetitive PET of nucleoside utilization and tumor proliferative activity with ^{18}F-FUdR or other suitable radiotracers can provide additional information about the localization of tumor responses to GCV therapy. PET with ^{18}F-FDG or ^{18}F-FET can be used as additional "surrogate" biomarkers of the treatment response, although these radiotracers are less sensitive than ^{18}F-FUdR for monitoring tumor responses to prodrug activation gene therapy of sarcomas with *HSV1-tk* and GCV.

ACKNOWLEDGMENTS

This research was supported by National Science Council grant NSC 94-3112-B-010-007 and Department of Health grant DOH 95-TD-G-111-021.

REFERENCES

1. Greco O, Dachs GU. Gene directed enzyme/prodrug therapy of cancer: historical appraisal and future perspectives. *J Cell Physiol.* 2001;187:22–36.
2. Moolten FL. Tumor chemosensitivity conferred by inserted herpes thymidine kinase genes: paradigm for a prospective cancer control strategy. *Cancer Res.* 1986;46:5276–5281.
3. Freeman SM, Abboud CN, Whartenby KA, et al. The "bystander effect": tumor regression when a fraction of the tumor mass is genetically modified. *Cancer Res.* 1993;53:5274–5283.
4. Culver KW, Ram Z, Wallbridge S, Ishii H, Oldfield EH, Blaese RM. In vivo gene transfer with retroviral vector-producer cells for treatment of experimental brain tumors. *Science.* 1992;256:1550–1552.
5. Ram Z, Culver KW, Oshiro EM, et al. Therapy of malignant brain tumors by intratumoral implantation of retroviral vector-producing cells. *Nat Med.* 1997;3:1354–1361.
6. Tjuvajev JG, Avril N, Oku T, et al. Imaging herpes virus thymidine kinase gene transfer and expression by positron emission tomography. *Cancer Res.* 1998;58:4333–4341.
7. Tjuvajev JG, Doubrovin M, Akhurst T, et al. Comparison of radiolabeled nucleoside probes (FIAU, FHBG, and FHPG) for PET imaging of HSV1-tk gene expression. *J Nucl Med.* 2002;43:1072–1083.
8. Alauddin MM, Shahinian A, Gordon EM, Bading JR, Conti PS. Preclinical evaluation of the penciclovir analog 9-(4-[^{18}F]fluoro-3-hydroxymethylbutyl)-guanine for in vivo measurement of suicide gene expression with PET. *J Nucl Med.* 2001;42:1682–1690.
9. Alauddin MM, Fissekis JD, Conti PS. A general synthesis of 2′-deoxy-2′-[^{18}F]fluoro-5-methyl-1-β-D-arabinofuranosyluracil and its 5-substituted nucleosides. *J Labelled Compds Radiopharm.* 2003;46:285–289.
10. Serganova I, Doubrovin M, Vider J, et al. Molecular imaging of temporal dynamics and spatial heterogeneity of hypoxia-inducible factor-1 signal transduction activity in tumors in living mice. *Cancer Res.* 2004;64:6101–6108.
11. Alauddin MM, Shahinian A, Park R, Tohme M, Fissekis JD, Conti PS. Synthesis of 2′-deoxy-2′-[^{18}F]fluoro-5-bromo-1-beta-D-arabinofuranosyluracil ([^{18}F]-FBAU) and 2′-deoxy-2′-[^{18}F]fluoro-5-chloro-1-beta-D-arabinofuranosyluracil ([^{18}F]-FCAU),

and their biological evaluation as markers for gene expression. *Nucl Med Biol.* 2004; 31:399–405.
12. Tjuvajev JG, Finn R, Watanabe K, et al. Noninvasive imaging of herpes virus thymidine kinase gene transfer and expression: a potential method for monitoring clinical gene therapy. *Cancer Res.* 1996;56:4087–4095.
13. Tjuvajev JG, Chen SH, Joshi A, et al. Imaging adenoviral-mediated herpes virus thymidine kinase gene transfer and expression in vivo. *Cancer Res.* 1999;59: 5186–5193.
14. Deng WP, Yang WK, Lai WF, et al. Non-invasive in vivo imaging with radiolabelled FIAU for monitoring cancer gene therapy using herpes simplex virus type 1 thymidine kinase and ganciclovir. *Eur J Nucl Med Mol Imaging.* 2004;31:99–109.
15. Jacobs A, Voges J, Reszka R, et al. Positron-emission tomography of vector-mediated gene expression in gene therapy for gliomas. *Lancet.* 2001;358:727–729.
16. Penuelas I, Mazzolini G, Boan JF, et al. Positron emission tomography imaging of adenoviral-mediated transgene expression in liver cancer patients. *Gastroenterology.* 2005;128:1787–1795.
17. Haberkorn U, Bellemann ME, Gerlach L, et al. Uncoupling of 2-fluoro-2-deoxyglucose transport and phosphorylation in rat hepatoma during gene therapy with HSV thymidine kinase. *Gene Ther.* 1998;5:880–887.
18. Miyagawa T, Oku T, Sasajima T, et al. Assessment of treatment response by autoradiography with ^{14}C-aminocyclopentane carboxylic acid, ^{67}Ga-DTPA, and ^{18}F-FDG in a herpes simplex virus thymidine kinase/ganciclovir brain tumor model. *J Nucl Med.* 2003;44:1845–1854.
19. Yaghoubi SS, Barrio JR, Namavari M, et al. Imaging progress of herpes simplex virus type 1 thymidine kinase suicide gene therapy in living subjects with positron emission tomography. *Cancer Gene Ther.* 2005;12:329–339.
20. Voges J, Reszka R, Gossmann A, et al. Imaging-guided convection-enhanced delivery and gene therapy of glioblastoma. *Ann Neurol.* 2003;54:479–487.
21. Delbeke D. Oncological applications of FDG PET imaging: brain tumors, colorectal cancer, lymphoma and melanoma. *J Nucl Med.* 1999;40:591–603.
22. Hoh CK, Seltzer MA, Franklin J, deKernion JB, Phelps ME, Belldegrun A. Positron emission tomography in urological oncology. *J Urol.* 1998;159: 347–356.
23. Shreve PD, Anzai Y, Wahl RL. Pitfalls in oncologic diagnosis with FDG PET imaging: physiologic and benign variants. *Radiographics.* 1999;19:61–77.
24. van Waarde A, Cobben DC, Suurmeijer AJ, et al. Selectivity of ^{18}F-FLT and ^{18}F-FDG for differentiating tumor from inflammation in a rodent model. *J Nucl Med.* 2004;45:695–700.
25. Weber WA. Use of PET for monitoring cancer therapy and for predicting outcome. *J Nucl Med.* 2005;46:983–995.
26. Hicks RJ. The role of PET in monitoring therapy. *Cancer Imaging.* 2005;5:51–57.
27. Weber WA, Wester HJ, Grosu AL, et al. O-(2-[^{18}F]Fluoroethyl)-L-tyrosine and L-[methyl-^{11}C]methionine uptake in brain tumours: initial results of a comparative study. *Eur J Nucl Med.* 2000;27:542–549.
28. Heiss P, Mayer S, Herz M, Wester HJ, Schwaiger M, Senekowitsch-Schmidtke R. Investigation of transport mechanism and uptake kinetics of O-(2-[^{18}F]fluoroethyl)-L-tyrosine in vitro and in vivo. *J Nucl Med.* 1999;40:1367–1373.
29. Pauleit D, Stoffels G, Schaden W, et al. PET with O-(2-^{18}F-fluoroethyl)-L-tyrosine in peripheral tumors: first clinical results. *J Nucl Med.* 2005;46:411–416.
30. Tsurumi Y, Kameyama M, Ishiwata K, et al. ^{18}F-Fluoro-2′-deoxyuridine as a tracer of nucleic acid metabolism in brain tumors. *J Neurosurg.* 1990;72:110–113.
31. Sato K, Kameyama M, Ishiwata K, Katakura R, Yoshimoto T. Metabolic changes of glioma following chemotherapy: an experimental study using four PET tracers. *J Neurooncol.* 1992;14:81–89.
32. Abe Y, Fukuda H, Ishiwata K, et al. Studies on ^{18}F-labeled pyrimidines: tumor uptakes of ^{18}F-5-fluorouracil, ^{18}F-5-fluorouridine, and ^{18}F-5-fluorodeoxyuridine in animals. *Eur J Nucl Med.* 1983;8:258–261.
33. Shiue CY, Arnett CD, Wolf AP. Syntheses of 5′-deoxy-5-[^{18}F]fluorouridine and related compounds as probes for measuring tissue proliferation in vivo. *J Labelled Comps Radiopharm.* 1984;21:865–873.
34. Ishiwata K, Monma M, Iwata R, et al. Automated synthesis of 5-[^{18}F]fluoro-2′-deoxyuridine. *Int J Appl Radiat Isot.* 1987;38:467–473.
35. Lemaire C, Damhaut P, Lauricella B, et al. Fast [^{18}F]FDG synthesis by alkaline hydrolysis on a low polarity solid phase support. *J Labelled Compds Radiopharm.* 2002;45:435–447.
36. Tjuvajev JG, Stockhammer G, Desai R, et al. Imaging the expression of transfected genes in vivo. *Cancer Res.* 1995;55:6126–6132.
37. Morin KW, Knaus EE, Wiebe LI, Xia H, McEwan AJ. Reporter gene imaging: effects of ganciclovir treatment on nucleoside uptake, hypoxia and perfusion in a murine gene therapy tumour model that expresses herpes simplex type-1 thymidine kinase. *Nucl Med Commun.* 2000;21:129–137.
38. Haberkorn U, Altmann A, Kamencic H, et al. Glucose transport and apoptosis after gene therapy with HSV thymidine kinase. *Eur J Nucl Med.* 2001;28:1690–1696.
39. Haberkorn U, Altmann A, Morr I, et al. Multitracer studies during gene therapy of hepatoma cells with HSV thymidine kinase and ganciclovir. *J Nucl Med.* 1997;38:1048–1054.

JNM The Journal of NUCLEAR MEDICINE

Molecular Imaging with ^{123}I-FIAU, ^{18}F-FUdR, ^{18}F-FET, and ^{18}F-FDG for Monitoring Herpes Simplex Virus Type 1 Thymidine Kinase and Ganciclovir Prodrug Activation Gene Therapy of Cancer

Hsin-Ell Wang, Hung-Man Yu, Ren-Shyan Liu, Mai Lin, Juri G. Gelovani, Jeng-Jong Hwang, Hon-Jian Wei and Win-Ping Deng

J Nucl Med. 2006;47:1161-1171.

The Journal of Nuclear Medicine is published monthly.
SNMMI | Society of Nuclear Medicine and Molecular Imaging
1850 Samuel Morse Drive, Reston, VA 20190.
(Print ISSN: 0161-5505, Online ISSN: 2159-662X)

SNMMI SOCIETY OF NUCLEAR MEDICINE AND MOLECULAR IMAGING